Finite element thermal analysis of an RCC dam

C. Aggarwal, Stantec Inc, India

This paper presents a two-dimensional (2D) finite element thermal analysis of a roller compacted concrete (RCC) dam. The thermal analysis of the dam demonstrates that temperature control during construction is critical to minimizing thermal stresses and preventing cracks. The results serve as a basis for optimizing construction schedules, implementing temperature control strategies, and ensuring long-term structural integrity and durability of the dam.

Thermal analysis of mass concrete structures, such as roller compacted concrete (RCC) dams, requires the evaluation of heat of hydration. This heat is generated during the exothermic reaction between cement and water. In mass concrete, the resulting thermal stresses can lead to detrimental cracking, and a subsequent reduction in mechanical properties. The need for heat of hydration analysis depends on factors such as structural dimensions, the type of structure, cement composition, and construction conditions.

The analysis presented in this paper is broadly categorized into two components: heat transfer analysis, and thermal stress analysis. Heat transfer analysis considers mechanisms such as conduction, convection, and internal heat generation. Thermal stress analysis considers temperature-dependent changes in material properties, including modulus of elasticity, creep, and shrinkage. These are influenced by curing conditions, temperature gradients, and concrete maturity. Surface cracking may occur because of temperature differentials between the surface and the core. In addition, through-cracks can develop when contraction during cooling is restrained by external boundary conditions, especially in high heat of hydration scenarios.

The most suitable method to assess temperature effects accurately during the construction stages involves non-linear incremental structural analysis (NISA). In this study, NISA is carried out using MIDAS FEA NX software.

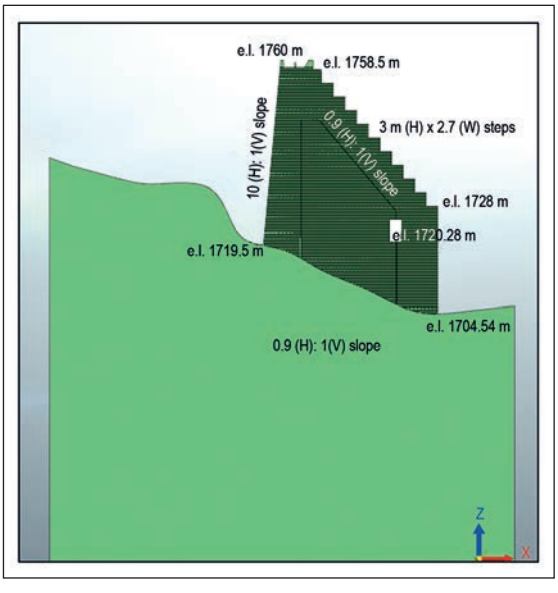

Fig. 1. The dam section taken for the analysis.

1. The NISA process

In the study the two dimensional (2D) non-linear, incremental, structural analysis (NISA) was carried out for the tallest section of an RCC dam. The dam section which was considered for the analysis is shown in Fig. 1.

2. Construction parameters

Differences in the way a monolith is constructed will impact the behaviour of a structure to varying degrees. The construction schedule adopted for the present study is shown in Table 1.

2.1 Lift heights

Since heat escape from a mass is inversely proportional to the square of its least dimension, and since the height of a lift will usually be the smallest dimension, the lift height can become a factor in the behaviour of a mass concrete structure. For the present analysis, a lift height of 3 m in one concrete pour was considered. Based on Table 1, the duration time for each lift was interpolated. A continuous concrete pour of one lift was assumed.

The time taken to pour each concrete lift will depend on the volume of concrete required for each pour. In the present analysis, a continuous concrete pour of 3 m lift height was assumed.

The remaining period of each lift is regarded as a waiting period before the pouring of the next lift. RCC dam construction is generally carried out over a relatively short timeframe with numerous lift joints (usually 300 mm to 600 mm in height).

Table 1: Construction schedule

Duration (days)	Elevation (m)	Lift (m)	Height from bottom (m)
0	1701.97	0.00	0.00
30	1708.43	6.46	6.46
60	1710.96	2.53	8.99
90	1713.06	2.11	11.10
120	1715.31	2.25	13.34
150	1717.42	2.11	15.45
180	1721.07	3.65	19.10
210	1724.86	3.79	22.89
240	1731.18	6.32	29.21
270	1735.25	4.07	33.29
300	1735.25	0.00	33.39
330	1743.26	8.01	41.39
360	1750.14	6.88	48.27

The durations adopted for each lift in the analysis are shown in Table 2.

With the MIDAS software, the time taken for each lift cycle can be simulated considering adequate time steps for every construction stage. A load factor of 1 can be assigned to the first step, and 0 to all the other steps in each construction stage to simulate the continuous pouring of one lift, and the remaining time as a waiting period before casting of the next lift.

2.3 Start time

The time of year at which an analysis is started can have a significant effect on the analytical results. A minimum of two NISAs should be performed using different start times. In the present analysis, two separate analysis have been performed, with start dates of 1 January and 1 June.

Changing the start date in the analysis requires the ambient temperature curve to be adjusted so that it corresponds to the time of year that the analysis begins.

Table 2: Lift heights taken for the analysis

Lift	Height (m)	Total height from bottom (m)	Total duration (days)	Days for casting lift	Construction stages
1	3	3	14	14.00	From 0 to 14 days
2	3	6	28	14.00	From 14 to 28 days
3	3	9	60	33.00	From 28 to 61 days
4	3	12	102	42.00	From 61 to 103 days
5	3	15	144	42.00	From 103 to 144 days
6	3	18	171	28.00	From 144 to 171 days
7	3	21	195	25.00	From 171 to 196 days
8	3	24	215	21.00	From 196 to 216 days
9	3	27	229	15.00	From 216 to 230 days
10	3	30	246	17.00	From 230 to 246 days
11	3	33	268	23.00	From 246 to 268 days
12	3	36	310	42.00	From 268 to 310 days
13	3	39	321	12.00	From 310 to 322 days
14	3	42	333	12.00	From 322 to 333 days
15	3	45	346	14.00	From 333 to 346 days
16	3	48	359	14.00	From 346 to 359 days
17	3	51	369	10.00	from 359 to 369 days
18	3	54	379	10.00	from 369 to 379 days

Table 3: Monthly temperature data

Month	Days in the month	Max. temp (ºC)	Min. temp (ºC)	Phase shift	Amplitude temp (ºC)	Midline temp in (ºC)	F (t) (ºC)
January	31	18.67	-3.167	0	10.9185	7.8	7.8
February	28	21.5	-2.5	0	12	9.5	9.5
March	31	25	-0.33	0	12.665	12.3	12.3
April	30	29.33	3.33	0	13	16.3	16.3
May	31	32.83	8.333	0	12.2485	20.6	20.6
June	30	35	12.8333	0	11.08335	23.9	23.9
July	31	35.67	15	0	10.335	25.3	25.3
August	31	35.67	15.67	0	10	25.7	25.7
September	30	33.83	13.167	0	10.3315	23.5	23.5
October	31	30	7.667	0	11.1665	18.8	18.8
November	30	23.83	2.167	0	10.8315	13.0	13.0
December	31	20.1667	-1.5	0	10.83335	9.3	9.3

F(t) = extreme ambient temperature function's monthly value (the midline of each month's max/min pair) used to build the 365 day sine function.

3. Climatic data

3.1 Extreme ambient temperature

The data required is the coldest monthly average temperature recorded for each month within any given year, and the hottest monthly average temperature recorded for each month within any given year. An extreme ambient temperature function should be developed as a sine wave with a 365-day period that captures the coldest and hottest of the extreme monthly average temperatures. The extreme ambient temperature is used to account for the possibility of seasons (months) having much higher or lower temperatures than the average ambient conditions developed using monthly averages based on multi-year averages.

Ambient function as a sine wave can be represented as:

$$D(t) = \text{Midline} - \text{Amplitude} \cdot \sin\left(\frac{2\pi}{\text{Period}} \cdot (t - \text{Phase shift})\right) \quad \text{... (1)}$$

The monthly maximum and minimum air temperatures shown in Table 3 were considered to develop the desired sine function.

3.2 Film coefficient

An essential part of heat transfer analysis is to model convection, which is the transfer of heat that occurs between a fluid (for example, air or water) and a concrete surface. The following equations are from the American Society of Heating, Refrigerating and Air Conditioning Engineers (ASHRAE) Handbook and Product Directory - 1977 Fundamentals [1977[1]]. These equations are used to calculate the film coefficients to be incorporated in finite element (FE) analysis for modelling convection. For surfaces without forms, the coefficients can be calculated based on the following:

$$h = 0.1132V^{0.8} \quad \text{for } V > 10.9 \text{ mph}$$

and:

$$h = 0.165 + 0.0513\,(V) \quad \text{for } V < 10.9 \text{ mph}$$

where:

$$h = \text{film coefficient}\ \left(\frac{Btu}{day\text{-}in.^{2\text{-}0}F}\right)$$

V = wind velocity (mph) ... (2)

Table 4: Monthly film coefficient

Month	Monthly average wind speed, *V* (km/h)	Film coefficient, h (W/m² ºC)	Film coefficient, h (J/m² day ºC)
January	2.242	8.05587339	696027.5
February	4.036	10.0040726	864351.9
March	5.733	11.8469344	1023575
April	7.04	13.2662746	1146206
May	7.559	13.829884	1194902
June	7.014	13.2380398	1143767
July	5.765	11.8816848	1026578
August	4.036	10.0040726	864351.9
September	2.242	8.05587339	696027.5
October	0.992	6.69843249	578744.6
November	0.25	5.89265557	509125.4
December	0.5	6.16414375	532582

Based on the data shown in Table 4, the ambient temperature curves and film coefficients shown in Table 5 have been used as inputs for different stages of construction for the considered two construction start dates.

3.3 Concrete placement temperature

For mass concrete structures, the temperature of the concrete at the time of placement is limited to control the temperature level within the mass caused by heat of hydration.

As with lift heights, if structural behaviour is acceptable, then consideration may be given to increasing the placement temperature. Increasing this temperature can lead to reduced costs because of decreased cooling requirements. Changing the placement temperature is a simple change to the initial conditions in the heat transfer analysis.

In FE analysis, the concrete placement temperature is provided as an initial temperature in analysis control for each construction stage.

Table 6 shows the concrete placement temperatures considered. These temperatures have been established through multiple trial analyses for each construction stage to ensure that the induced tensile stresses remain within, or as close as possible, to the allowable limits.

4. Material properties

Information on the thermal, mechanical, and physical properties are required for concrete mixtures, foundation materials, and air. Some of these properties are time dependent, while others are assumed to remain constant with respect to time. Fig. 2 shows the proposed zoning of the RCC dam section under consideration.

Table 5: Input ambient temperature curve and film coefficient

Construction stage	Constructed dam crest elevation (m)	Ambient temp curve (1 Jan start date)	Film coefficient in j/m² day ºC (1 Jan start date)	Ambient temp curve (1 June start date)	Film coefficient in j/m² day ºC (1 June start date)	Ambient temp curve (1 Oct start date)	Film coefficient in j/m² day ºC (1 Oct start date)
From 0 to 14 days	1707.5	Jan	696027.5	Jun	1143766.6	Oct	578744.6
From 14 to 28 days	1710.5	Jan	696027.5	Jun	1143766.6	Oct	578744.6
From 28 to 61 days	1713.5	Feb	864351.9	Jul	1026577.6	Nov	509125.4
From 61 to 103 days	1716.5	Mar	1023575.1	Aug	864351.9	Dec	532582.0
From 103 to 144 days	1719.5	Apr	1146206.1	Sep	696027.5	Jan	696027.5
From 144 to 171 days	1722.5	May	1194902.0	Oct	578744.6	Feb	864351.9
From 171 to 196 days	1722.5	June	1143766.6	Nov	509125.4	Mar	1023575.1
From 196 to 216 days	1728.5	July	1026577.6	Dec	532582.0	Apr	1146206.1
From 216 to 230 days	1731.5	Aug	864351.9	Jan	696027.5	May	1194902.0
From 230 to 246 days	1734.5	Aug	864351.9	Feb	864351.9	May	1194902.0
From 246 to 268 days	1737.5	Sep	696027.5	Mar	1023575.1	Jun	1143766.6
From 268 to 310 days	1740.5	Oct	578744.6	Apr	1146206.1	Jul	1026577.6
From 310 to 322 days	1743.5	Nov	509125.4	May	1194902.0	Aug	864351.9
From 322 to 333 days	1746.5	Nov	509125.4	May	1194902.0	Aug	864351.9
From 333 to 346 days	1749.5	Nov	509125.4	May	1194902.0	Aug	864351.9
From 346 to 359 days	1752.5	Dec	532582.0	Jun	1143766.6	Sep	696027.5
From 359 to 369 days	1755.5	Jan	532582.0	Jun	1143766.6	Sep	696027.5
From 369 to 379 days	1758.5	Jan	532582.0	Jun	1143766.6	Sep	696027.5

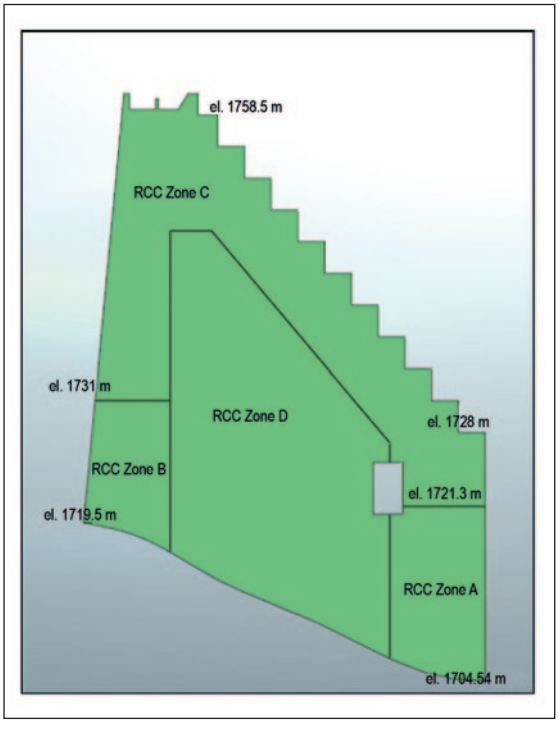

Fig. 2. RCC zoning of the dam section.

4.1 Concrete properties

The following thermal, mechanical and physical properties, as shown below must be determined as NISA inputs.

4.1.1 Thermal properties

The thermal properties for sulphate resistant cement (SRC) considered in the present analysis are summarized in Table 7.

4.1.2 Adiabatic temperature rise

An adiabatic system is a system in which heat is not allowed to enter or leave. The adiabatic temperature rise, therefore, is the change in temperature caused by hydration of the cementitious materials in a concrete mass when adiabatic conditions exist. It is a measure of the heat evolution of the concrete mixture, and serves as the loading in the heat transfer analyses.

The design heat of hydration curve has been defined assuming that heat generated at 7 and 28 days is approximately 65 per cent and 75 per cent of the ultimate heat of hydration, respectively. The design heat of hydration curve used here is shown in Fig. 3.

The adiabatic temperature rise of the RCC mixes used in the dam body has been evaluated according to the Eq. 3.

Table 6: Concrete placement temperatures in the study

Construction stages	Constructed dam crest elevation (m)	1 Jan start date: maximum placing temperature (ºC)	1 June start date: maximum placing temperature (ºC)
From 0 to 14 days	1707.5	8	22
From 14 to 28 days	1710.5	8	22
From 28 to 61 days	1713.5	8	23
From 61 to 103 days	1716.5	5	20
From 103 to 144 days	1719.5	8	18
From 144 to 171 days	1722.5	22	18
From 171 to 196 days	1725.5	22	18
From 196 to 216 days	1728.5	23	12
From 216 to 230 days	1731.5	20	15
From 230 to 246 days	1734.5	20	15
From 246 to 268 days	1737.5	18	18
From 268 to 310 days	1740.5	18	15
From 310 to 322 days	1743.5	18	22
From 322 to 333 days	1746.5	18	22
From 333 to 346 days	1749.5	18	22
From 346 to 359 days	1752.5	12	22
From 359 to 369 days	1755.5	8	22
From 369 to 379 days	1758.5	8	22

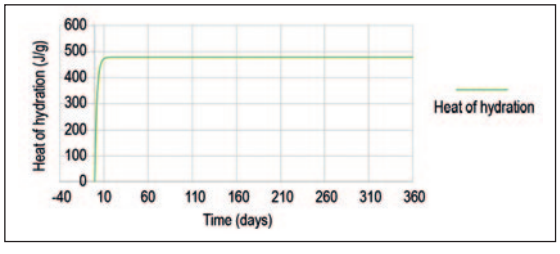

Fig. 3. Design heat of hydration curve.

$$T_{AD}(t) = \frac{H(t)\ (C + k\ F)}{c \cdot \rho} \quad \text{... (3)}$$

where:
$TAD(t)$ = adiabatic temperature rise at time t (˚C);
$H(t)$ = heat of hydration liberated by the cement at time t (J/g);
C = cement content (kg/m^3); and,
F = flyash content (kg/m^3).

Table 7: Considered thermal properties for SRC

Cementitious material	RCC zone	Cement content (kg/m^3)	Flyash content (kg/m^3)	Contribution of flyash to heat of hydration	Specific heat of RCC (kJ/kgºC)	Density of RCC (kg/m^3)	Thermal diffusivity (m^2/h)	Thermal conductivity (W/mºC)	Thermal coefficient (×10^6/ºC)
SRC	A	180	0	0.5	0.9	2400	0.00425	2.550002	8
SRC	B	145	0	0.5	0.9	2400	0.00425	2.550002	8
SRC	C	115	0	0.5	0.9	2400	0.00425	2.550002	8
SRC	D	85	0	0.5	0.9	2400	0.00425	2.550002	8

SRC calorimetry gave $H_u \approx 479$ J/g and $m = 0.422$ (with 7- and 28 day points at ≈ 65 per cent and ≈ 75 per cent of H_u). Using zone cement contents with fly ash contribution factor 0.5, the maximum adiabatic rises are: Zone A, 39.9 ˚C; Zone B, 32.15 ˚C; Zone C, 25.5 ˚C; and, Zone D 18.84 ˚C.

The maximum adiabatic rise in temperate is evaluated as 39.9˚C for Zone A, 32.15 ˚C for Zone B, 25.5 ˚C for Zone C and 18.84 ˚C for Zone D.

Another parameter, the relative velocity coefficient (sometimes called reactive velocity coefficient, hardening rate coefficient, or rate parameter) controls how fast the heat of hydration develops over time. For sulphate resistant cement (SRC) relative velocity coefficient of 0.3 to 0.45 is commonly used. In the present analysis, 0.442 is used based on laboratory test results of the cement. Based on above data, heat source functions for different zones of concrete are considered in FE analysis.

4.2 Mechanical properties

Time-dependent compressive strength, relative humidity, shrinkage and creep are required for heat of hydration analysis. Time functions for these properties are built into the MIDAS software for various international codes. In the present analysis CEB-FIP Model Code 1990, [1993[2]] is used to define the input time functions for these properties.

4.2.1 Compressive strength

Normal hardening cement was assumed for the RCC zones. The input curve shown in Fig. 4 for time dependent compressive strengths is considered for the analysis as per CEB-FIP Model Code 1990, [1993[2]].

4.2.2 Modulus of elasticity

For practical purposes, only the deformation that occurs during loading is considered to contribute to the strain in calculating the modulus of elasticity. Subsequent increases in strain caused by sustained loading are referred to as creep. The modulus of elasticity is a function of the degree of hydration and is therefore time dependent (see Fig. 5).

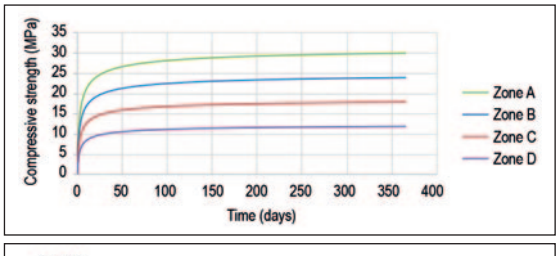

Fig. 4. Compressive strength curve for different zones of the RCC.

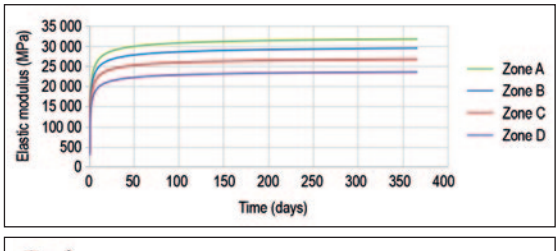

Fig. 5. Elastic modulus curve for different zones of the RCC.

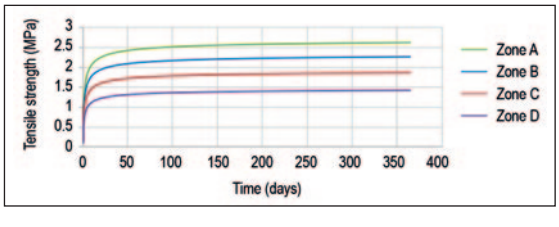

Fig. 6. Tensile strength curve for different zones of the RCC.

4.2.3 Tensile capacity

The cracking resistance of concrete is determined by a combination of limiting tensile strain and tensile stress. These properties are dependent on time and the rate of loading (see Fig. 6).

4.2.4 Creep

Creep is defined as time-dependent deformation caused by sustained load. For the purposes of a NISA, five ages of loading were conducted: 1 day, 3 days, 14 days, 60 days and 365 days. A creep curve, as per CEB FIP 1990 [1993[2]], was considered in the FE analysis for the different zones of concrete. Relative humidity of 70 per cent was considered as an input to plot creep and shrinkage curves.

4.2.5 Autogenous shrinkage

Autogenous shrinkage is a decrease in the volume of a concrete specimen or member caused by hydration of the cementitious materials without the concrete gaining or losing moisture. This type of volume change occurs in the interior of a large mass of concrete. This property is modelled as a function of time as per CEB FIP 1990 [1993[2]] in the analyses for different zones of concrete.

4.2.6 Crack ratio

NISA is based on an interactive stress-strain cracking criterion. The basis for the criterion is data from the slow load test. The aging modulus of elasticity makes the cracking criterion age dependent. The MIDAS software checks the time-dependent ratios of the allowable tensile stresses to the resulting tensile stresses (crack ratios) of individual nodes resulting from heat of hydration stage analysis in contours at each time step. Age-dependent elastic modulus, compressive strength, tensile strength, creep, and shrinkage as per CEB FIP 1990 [1993[2]] mentioned earlier, are provided in the software for the analysis.

5. Foundation properties

Foundation properties should be included in the heat transfer model to determine a realistic temperature distribution within the structure. Rock foundations extending up to about the dam height in a vertical direction were modelled. Ideally, prior to carrying out the heat transfer analysis of the structure and foundation, a heat transfer analysis should be performed on the foundation for a one year period, to determine the temperature distribution in the foundation for the start of concrete placement. In the present analysis, because of the absence of heat transfer

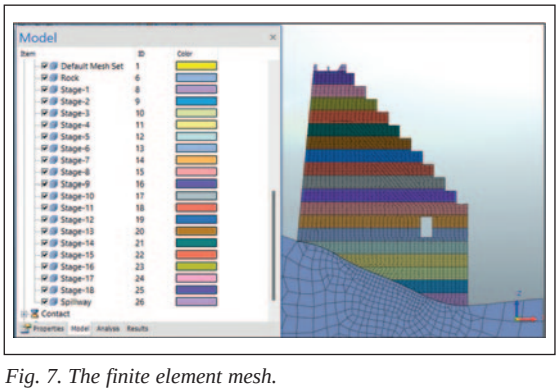

Fig. 7. The finite element mesh.

data for the foundation, thermal diffusivity has been assumed to be equal to that of the concrete. The yearly ambient temperature and film coefficient curves have been used to define the initial foundation temperature for each construction stage. These curves have been adjusted according to the construction start date in the analysis. In the absence of site-specific measurements, the foundation thermal diffusivity was assumed equal to that of the adjacent RCC zones for initialization; yearly ambient curves were used to set stage-wise initial foundation temperatures.

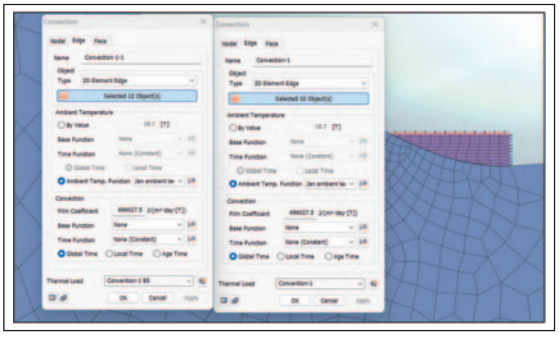

Fig. 8. Convection load applied in the first stage of construction.

Table 8: Analysis results

Construction stages	Constructed dam top level	Maximum induced temperature (ºC)		Maximum induced principal stresses after lift pour (MPa)		Minimum crack ratio (allowable tension/ induced tension)		Crack ratio check 1 Jan start date		Crack ratio check 1 June start date	
		1 Jan start date	1 June start date	1 Jan start date	1 June start date	1 Jan start date	1 June start date	Construction month	Crack check	Construction month	Crack check
From 0 to 14 days	1707.5	42.2	56.3	0.7	0.7	1.7	1.6	Jan	Crack ratio >1, safe	Jun	Crack ratio >1, safe
From 14 to 28 days	1710.5	41.8	55.6	1.4	1.3	1.1	1.1	Jan	Crack ratio >1, safe	Jun	Crack ratio >1, safe
From 28 to 61 days	1713.5	41.2	55.9	2.4	2.3	~1	~1	Feb	Crack ratio ~ =1, safe	Jul	Crack ratio ~ =1, safe
From 61 to 103 days	1716.5	38.2	53.2	1.7	1.7	1.0	~1	Mar	Crack ratio ~ =1, safe	Aug	Crack ratio ~ =1, safe
From 103 to 144 days	1719.5	40.8	51.5	1.5	1.6	1.0	1.0	Apr	Crack ratio ~ =1, safe	Sep	Crack ratio >1, safe
From 144 to 171 days	1722.5	47.2	48.7	1.6	1.6	1.3	1.3	May	Crack ratio >1, safe	Oct	Crack ratio >1, safe
From 171 to 196 days	1725.5	46.3	44.5	1.1	0.9	1.7	1.6	Jun	Crack ratio >1, safe	Nov	Crack ratio >1, safe
From 196 to 216 days	1728.5	48.3	39.6	1.5	2.5	0.9	0.6	Jul	Crack ratio <1 at 1 node of gallery edge, after ignoring gallery edges, crack ratio >1, safe	Dec	Crack ratio <0.6 at 1 node of gallery edge, after ignoring gallery edges, min crack ratio ~1, safe
From 216 to 230 days	1731.5	47.2	40.5	1.0	1.2	1.9	1.1	Aug	Crack ratio >1, safe	Jan	Crack ratio >1, safe
From 230 to 246 days	1734.5	43.1	36.1	1.0	1.6	1.4	1.1	Aug	Crack ratio >1, safe	Feb	Crack ratio >1, safe
From 246 to 268 days	1737.5	40.8	37.9	1.1	1.2	1.4	1.2	Sep	Crack ratio >1, safe	Mar	Crack ratio >1, safe
From 268 to 310 days	1740.5	39.5	35.1	1.0	1.4	1.2	1.0	Oct	Crack ratio >1, safe	Apr	Crack ratio ~ =1, safe
From 310 to 322 days	1743.5	38.9	41.7	1.0	1.1	1.5	1.3	Nov	Crack ratio >1, safe	May	Crack ratio >1, safe
From 322 to 333 days	1746.5	39.2	42.9	1.1	1.1	1.4	1.2	Nov	Crack ratio >1, safe	May	Crack ratio >1, safe
From 333 to 346 days	1749.5	39.2	43.0	1.2	1.1	1.4	1.3	Nov	Crack ratio >1, safe	May	Crack ratio >1, safe
From 346 to 359 days	1752.5	35.7	44.8	1.2	1.1	1.3	1.3	Dec	Crack ratio >1, safe	Jun	Crack ratio >1, safe
From 359 to 369 days	1755.5	33.6	45.3	1.2	1.1	1.3	1.3	Jan	Crack ratio >1, safe	Jun	Crack ratio >1, safe
From 369 to 379 days	1758.5	33.4	45.5	1.2	1.2	1.2	1.3	Jan	Crack ratio >1, safe	Jun	Crack ratio >1, safe
Spillway	1760.0	33.1	44.1	1.6	1.6	0.9	0.9	Jan	Crack ratio ~ <1, slightly unsafe	Jun	Crack ratio ~ <1, slightly unsafe

Gallery edge refers to internal gallery perimeter nodes that exhibit localized stress concentrations. Crack-ratio screening treats isolated edge nodes as non-governing if the contiguous field satisfies crack ratio ≥ 1.0. Where a single edge node showed crack ratio 0.6 to 0.9, adjacent nodes and the field average met the criterion; therefore the stage is classified safe.

6. FE analysis

The construction stage analysis considered varied pouring sequences and environmental conditions, ensuring comprehensive analysis and safety.

6.1 Finite element mesh and pouring stages

The FE model shown in Fig. 7 has been developed using MIDAS software for 2D plane strain thermal analysis of an RCC dam.

RCC mesh elements are named as per their pouring sequence. The lift height of each concrete pour is considered as 3 m.

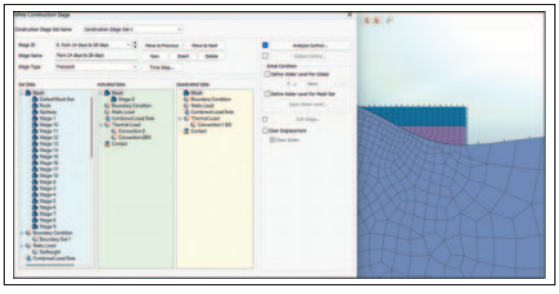

Fig. 9. Convection load applied in the second stage of construction.

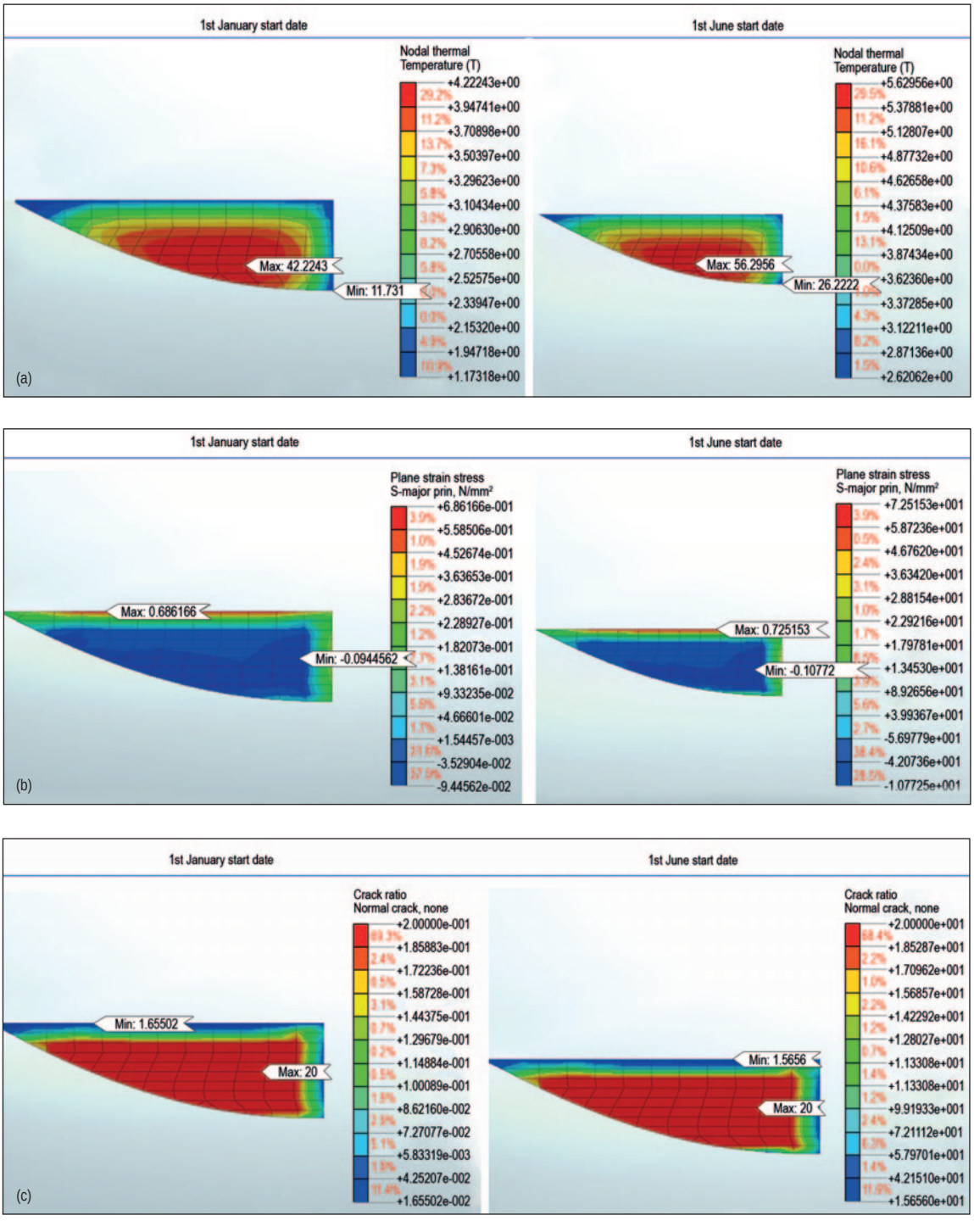

Figs. 10(a-c): Start of construction (Stage 1) – (a) temperature field; (b) principal tensile stress contours; (c) crack-ratio contours.

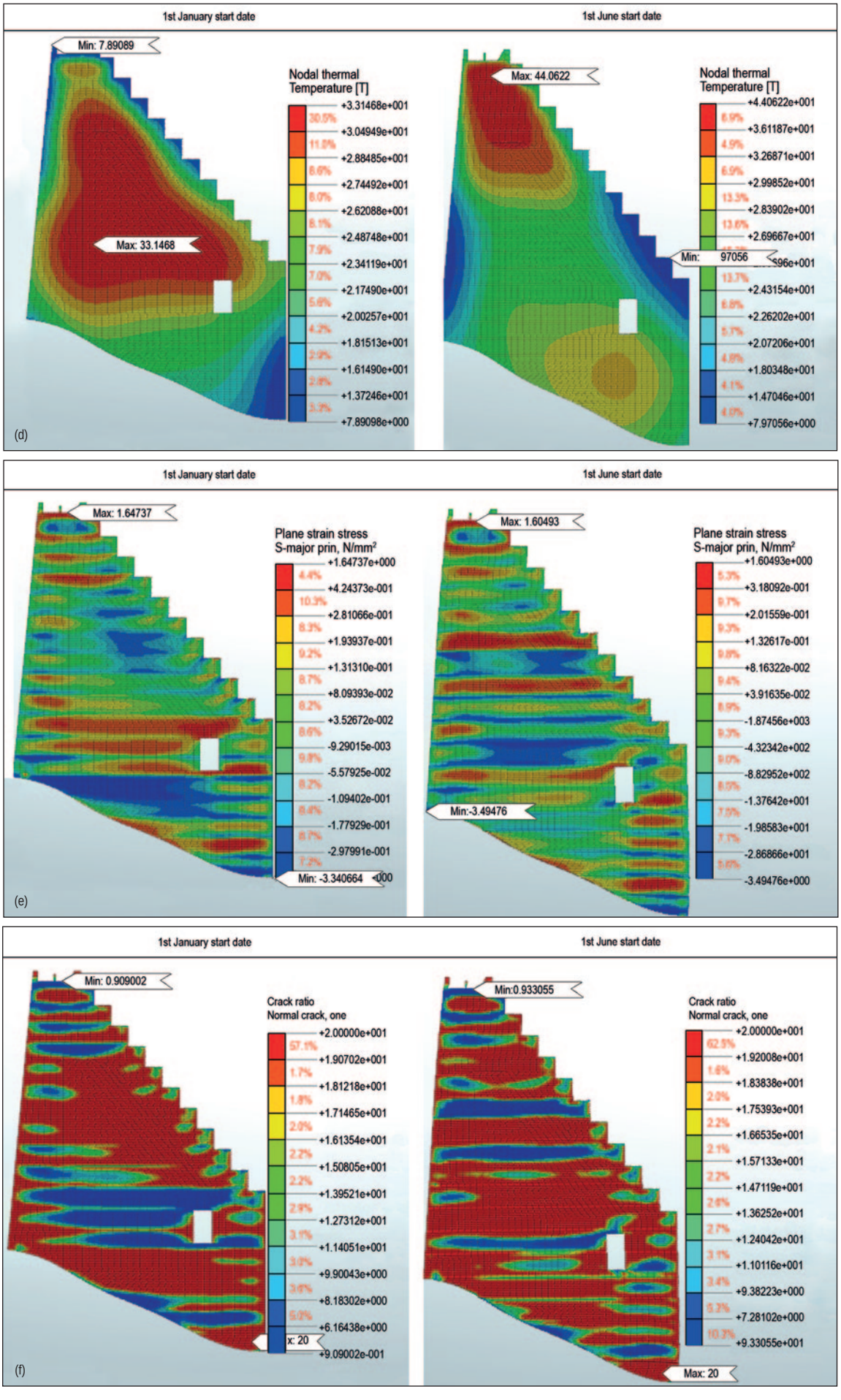

Figs. 10(d–f): End of construction (final stage) — (d) temperature field; (e) principal tensile stress contours; (f) crack-ratio contours. In (c,f), crack-ratio ≥ 1.0 indicates no thermal cracking.

6.2 Thermal load application

The heat of hydration for different concrete zones is applied as a zone wise heat source function, defined from the design heat of hydration curve and the zone mixes, calibrated using $H(t) = H_u (1 - e^{-mt})$ with $m = 0.422$ derived from SRC test data. The ambient temperature is modelled as a convection load on the exposed faces of each activated mesh set during every construction stage. For mesh edges that will be covered by subsequent concrete pours, the convection load is deactivated in the next stage. Consequently, two sets of convection loads are applied in each stage: one on edges that remain exposed throughout construction, and another on edges that will later be covered by concrete.

Fig. 8 illustrates the application of two sets of convection loads in Construction Stage 1. The right-side edge of the Stage-1 mesh set will remain permanently exposed to the atmosphere, while the top edge will be covered in the subsequent stage. Convection-1 BS is the convection load applied on the top edge of the mesh set.

In the second construction stage, the convection load 'Convection-1 BS' is deactivated, and the loads corresponding to Construction Stage 2 are applied, as shown in Fig. 9.

Similarly, all subsequent construction stages are simulated.

The results of the analysis are shown in Table 8.

Temperature distribution, principal stresses and crack ratio results of the first and last stages of construction are shown in Figs. 10(a) to 10(f).

7. Conclusion

The thermal analysis of the RCC dam demonstrates that temperature control during construction is critical to minimizing thermal stresses and preventing cracking.

By simulating heat of hydration, ambient temperature variations, and convection effects across different construction stages, the analysis ensures that induced tensile stresses remain within allowable limits.

The application of staged thermal loads, combined with appropriate boundary conditions, provides a realistic representation of temperature evolution throughout the dam.

These results serve as a basis for optimizing construction schedules, implementing temperature control strategies, and ensuring long-term structural integrity and durability of the dam. Results for 1 January and 1 June start dates confirm lower crack-risk staging for a summer initiation, whereas April is unfavourable because of the largest 24-hour ambient swing (≈3 °C to ≈30 °C), which increases early-age thermal gradients. ◊

References

1. **American Society of Heating, Refrigerating and Air Conditioning Engineers (ASHRAE)**, "Handbook and Product Directory 1977 Fundamentals"; 1977.
2. **Comité Euro-International du Béton**, "CEB-FIP Model Code 1990"; 1993.

Bibliography

US Army Corps of Engineers, "Gravity dam design", EM 1110-2-2200; 1995.

US Army Corps of Engineers, "Nonlinear incremental structural analysis of Zintel Canyon Dam," ETL 1110-2-536; 1994.

C. Aggarwal

Chetan Aggarwal is a Principal Civil Engineer at Stantec Inc, based in India, and specializing in the design and analysis of large-scale concrete hydropower structures such as dams, powerhouses, turbine generator foundations, and underground caverns. His expertise includes finite element modelling (FEM), static and dynamic structural analysis, seismic time-history analysis, heat of hydration modelling, thermal analysis, construction stage simulation, and stress evaluation under time-dependent effects. He is proficient in advanced engineering software tools, such as MIDAS FEA NX, and applies international standards including USACE Engineering Manuals, Indian codes, European codes, and Australian codes. Chetan focuses on optimizing structural design to ensure integrity and durability in complex infrastructure projects.

Stantec Inc, Amar Tech Park, 7th and 8th Floor,
802, Patil Nagar, Balewadi, Pune, Maharashtra 411045, India.